†Electronic supporting information

Dopant-free band edge shift in $BiVO_4$ particles for enhanced oxygen evolution under simulated sunlight

Niqab Khan,*[a] Rogério Nunes Wolff,[a] Hameed Ullah,[a] Gustavo J. Chacón,[b] Washington Santa Rosa,[c] Jairton Dupont,[b] Renato Vitalino Gonçalves,[c] Sherdil Khan,*[a]

[a] Laboratory of Nanomaterials for Renewable Energy and Artificial Photosynthesis (NanoREAP), Programa de Pós-Graduação em Física (PPGFis), Federal University of Rio Grande do Sul (UFRGS), Campus do Vale, Agronomia, Porto Alegre-RS, Brazil.

[b] Laboratory of Molecular Catalysis (LAMOCA), Programa de Pós-Graduação em Química (PPQ), Federal University of Rio Grande do Sul (UFRGS), Campus do Vale, Agronomia, Porto Alegre-RS, Brazil.

[c] Laboratory of Artificial Photosynthesis (LAPA), Institute of Physics of São Carlos, University of São Paulo (USP), São Paulo, Brazil.

* sherdil.khan@ufrgs.br

Table S1. Crystalline (based on XRD analyses) and morphological (based on SEM images) properties of synthesized $BiVO_4$ through [BMIm] and [M(MOE)Im] based ionic liquids.

Sample	Crystallite size (nm)	Crystallinity (100%)	Particle size (nm)
Pure $BiVO_4$	11	54	2725±86
Bi:[V-Bm]	18	86	221±30
Bi:[V-Me]	18	76	980±62
[Bi-Bm]:[V-Bm]	19	*	1733±72
[Bi-Me]:[V-Me]	19	*	3236±47

**Additional peaks of V_2O_5 were observed which affect the crystallinity (%) calculations; therefore, their crystallinity was not calculated.*

Table S2. Raman shift and (V-O) bond length (Figure S4), surface area (Figure S4), bandgap (Figure 2c), V/B ratio (Figure 4) and oxygen evolution (Figure 5) of synthesized $BiVO_4$ with different ionic liquids

Entry	Sample	Raman shift (cm^{-1})	V-O length (Å)	S_{BET} (m^2/g)	Bandgap (eV)	V/B ratio	O_2 Evolution (µmol)
1	Bi:[V-Bm]	826.67	1.6961	11.43	2.41	0.51	28.6
2	[Bi-Bm]:[V-Bm]	828.24	1.6950	11.66	2.25	1.56	16.6
3	Bi:[V-Me]	824.90	1.6971	11.79	2.37	0.69	24.2
4	[Bi-Me]:[V-Me]	827.63	1.6955	11.10	2.29	1.72	3.2
5	Pure $BiVO_4$	828.91	1.6947	*	2.44	0.64	10.3

*Less than the instrument limit.

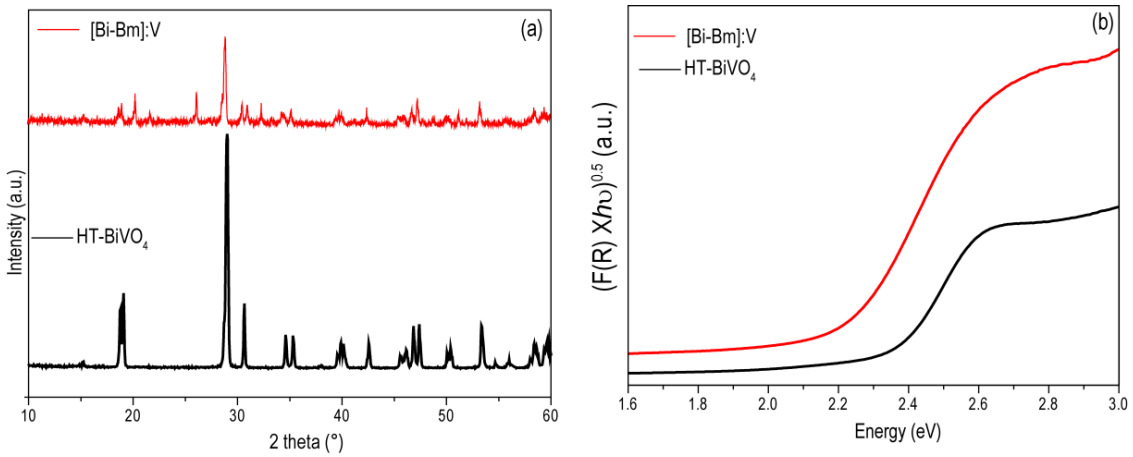

Figure S1. (a) XRD patterns and (b) UV –Vis diffused reflectance of [Bi-Bm]:V in which [BMIm] based IL anchored Bi was mixed with NH_4VO_3 to form $BiVO_4$ and HT-$BiVO_4$ prepared by conventional hydrothermal process.

Figure S1 displays the XRD patterns of [Bi-Bm]:V and HT-$BiVO_4$. For [Bi-Bm]:V in addition to $BiVO_4$ ((JCPDS) Card No. 14-0688), peaks at 2θ ~ 20°, 26° and 31° were also observed which correspond to V_2O_5. Furthermore, as compared to [Bi-Bm]:[V-Bm], and [Bi-Me]:[V-Me] (Figure 2), the relative peaks intensities of V_2O_5 was higher for [Bi-Bm]:V, indicating the formation of larger content of V_2O_5. Thus, anchoring IL with Bi side for the formation of $BiVO_4$ strongly decreases the diffusibility of Bi with V for the complete formation of $BiVO_4$. However, this synthesis results in large O defects,

thereby a notable red-shift in the bandgap was clearly observed as compared to HT-$BiVO_4$ (Figure S1b) and pure $BiVO_4$ (Figure 5).

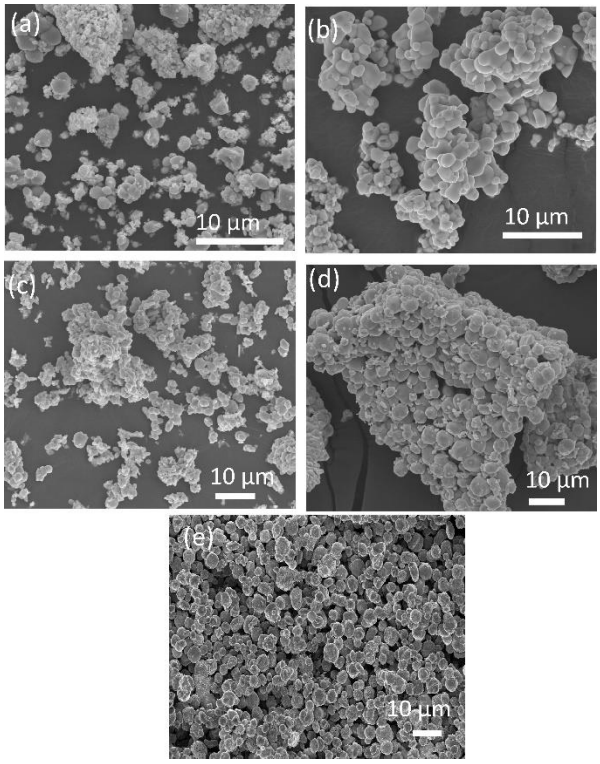

Figure S2. SEM images of the synthesized samples with and without ionic liquid. (a) Bi:[V-Bm], (b) Bi:[V-Me], (c) [Bi-Bm]:[V-Bm], (d) [Bi-Me]:[V-Me] and (e) Pure $BiVO_4$.

Figure S2 compares the low magnification images of the prepared samples, the higher magnification SEM are presented in Figure 3. As compared to pure $BiVO_4$, the samples prepared by IL presents smooth particles.

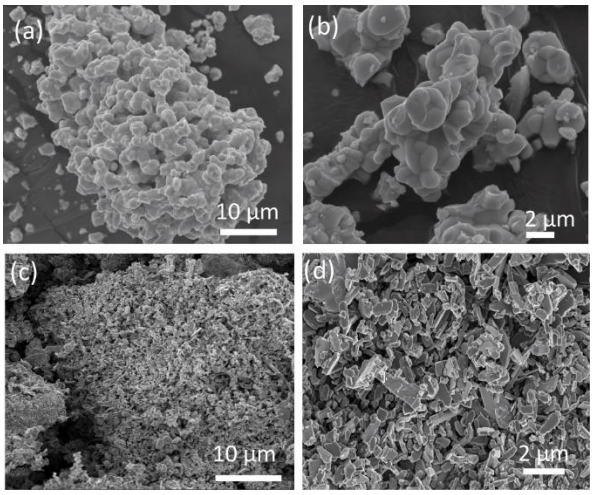

Figure S3, SEM images of (a-b) [Bi-Bm]:V in which [BMIm] based IL anchored Bi was mixed with NH_4VO_3 to form $BiVO_4$ and (c-d) HT-$BiVO_4$ prepared by conventional hydrothermal process.

Figure S3 (a-b) displays the SEM images of HT-$BiVO_4$; showing the obtained morphology is agglomerated microparticles. IL based synthesized [Bi-Bm]:V resulted into a totally different morphology (Figure S2 (c,d)) than HT-$BiVO_4$ and also as compared to all other samples (Figure 3).

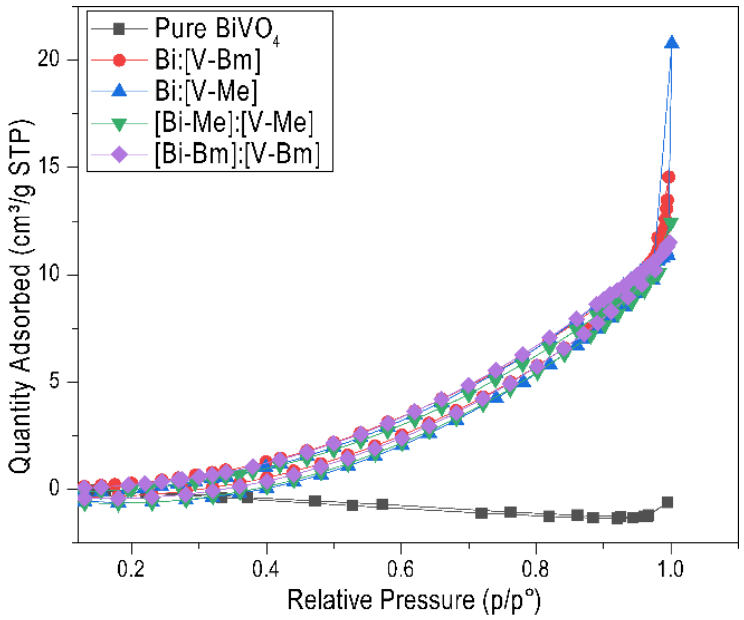

Figure S4. BET adsorption-desorption isotherms of the samples prepared with and without IL.

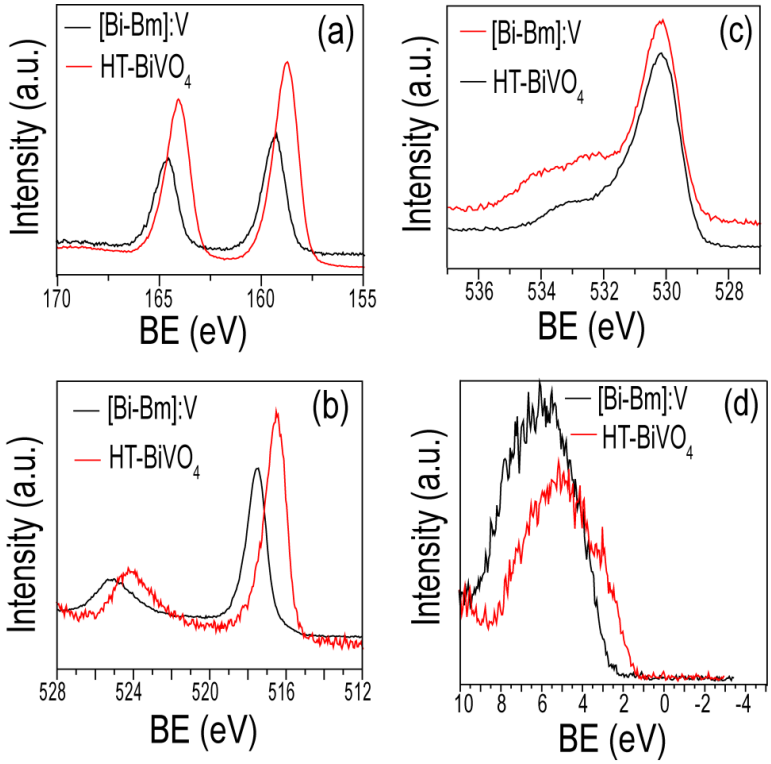

Figure S5. XPS spectra of the (a) Bi 4f, (b) V 2p and (c) O 1s core levels of [Bi-Bm]:V and HT-$BiVO_4$ and (d) their respective VB spectra. A clear peak shift in Bi df, V2p and VB can be observed for [Bi-Bm]:V as compared to HT-$BiVO_4$.

Figure S5 displays XPS spectra of [Bi-Bm]:V and HT-$BiVO_4$. The peaks positions of HT-$BiVO_4$ does not differ from pure $BiVO_4$ (Figure 4). A clear blue-shift is observed for [Bi-Bm]:V as compared to HT-$BiVO_4$ for Bi 4f, V2p and VB spectra. These results also agree with Figure 5 where blue-shift was clearly observed for IL based syntheses as compared to pure $BiVO_4$. In addition, the O1s spectra of [Bi-Bm]:V (Figure S1c) is also similar to [Bi-Bm]:[V-Bm] and [Bi-Me]:[V-Me] which present an additional peak at BE~533.2 eV corresponding to chemisorbed oxygen species. Hence anchoring IL to Bi side improves the light abosrbption by upshifting the VB but with a drawback of low reactivity of Bi with V and accumulation of O species on $BiVO_4$ surface.

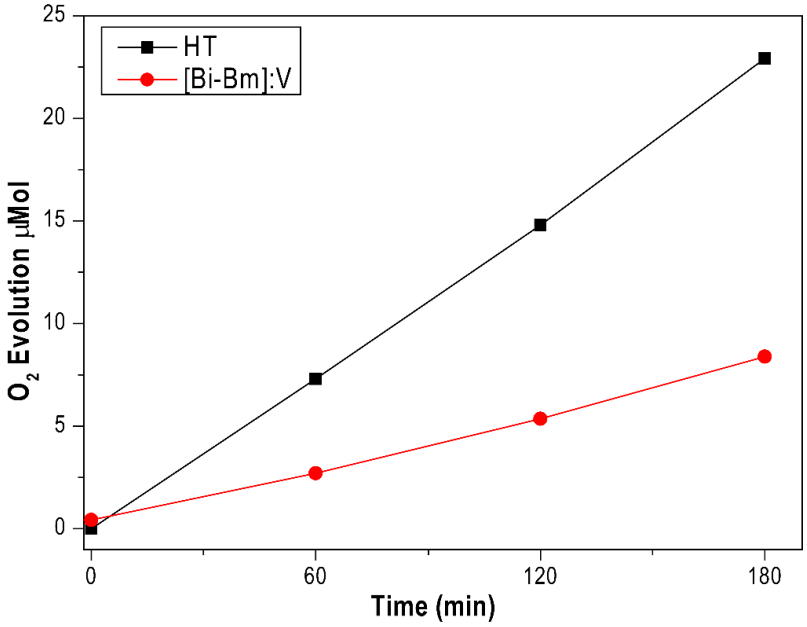

Figure S6. Oxygen evolution of [Bi-Bm]:V and HT-$BiVO_4$ for 3h exposure to 300 W Xe radiations filtered with AM 1.5G.

Figure S4 displays oxygen evolution of [Bi-Bm]:V and HT-$BiVO_4$ under simulated sunlight. Though [Bi-Bm]:V presented large absorption in the visible light, however due to accumulation of O species and presence of V_2O_5 could not perform better as compared to HT-$BiVO_4$ and pure $BiVO_4$ (Figure 5a).

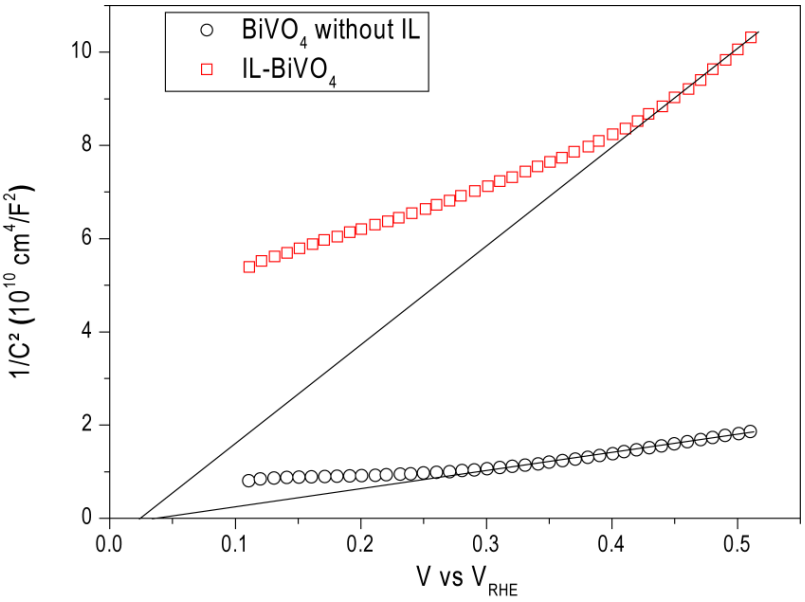

Figure S7. Mott-Schottky plots of $BiVO_4$ (prepared without IL) and BMIm-$BiVO_4$ prepared by BMIm based IL.

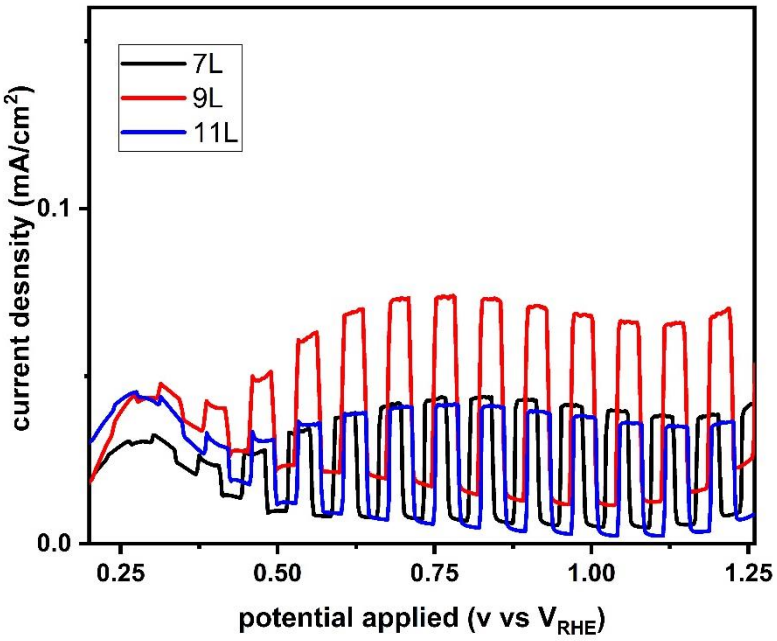

Figure S8. Chopped LSV curves of Bi:[V-Bm] with different layers i.e. 7L, 9L and 11L under 1 Sun illumination.

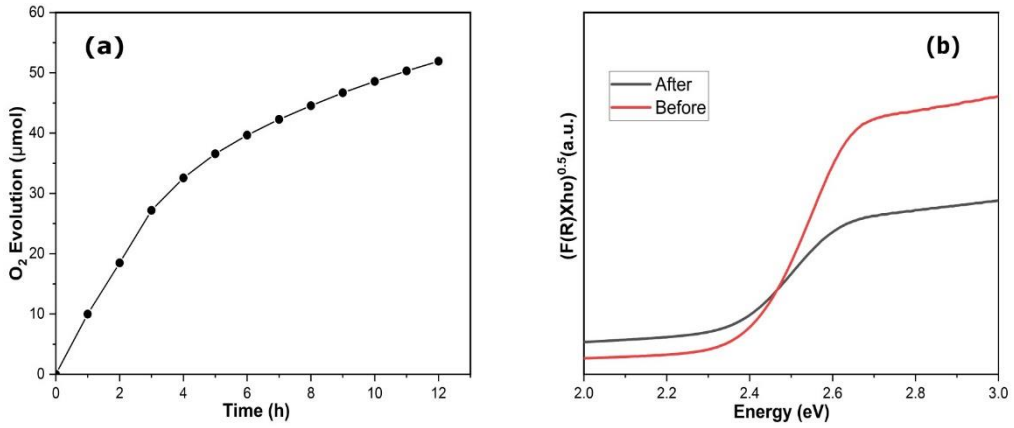

Figure S9: (a) Long time photochemical water oxidation activity of Bi:[V-Bm] at AM 1.5 illumination in 0.05 M of $Fe(NO_3)_3.9H_2O$. (b) UV –Vis diffused reflectance of Bi:[V-Bm] before and after 12h photocatalytic oxygen evolution test.